Available online at www.sciencedirect.com
ScienceDirect
Ceramics International 37 (2011) 2643–2654
CERAMICS INTERNATIONAL
www.elsevier.com/locate/ceramint

The sintering kinetics of ultrafine tungsten carbide powders

A.K. Nanda Kumar [a,*], M. Watabe [b], K. Kurokawa [a]

[a] *Laboratory of High Temperature Materials, Centre for Advanced Research of Energy and Materials, Faculty of Engineering, Hokkaido University, Japan*
[b] *Ohta Seiki Co. Ltd., Japan*

Received 17 January 2011; received in revised form 19 March 2011; accepted 7 April 2011
Available online 14 April 2011

Abstract

The sintering kinetics of nano grained tungsten carbide (*n*-WC) powders has been analyzed by non isothermal and isothermal sintering. Non isothermal sintering experiments reveal a multi staged sintering process in which at least three major sub-stages can be distinguished. The isothermal shrinkage strain also exhibits an asymptotic behavior with time indicating an end point density phenomenon in most of the temperature ranges. Combined microstructural and kinetic data analyses suggest that differences in the sinterability of inter and intra agglomerate pore phases introduce sub-stages in the sintering process which manifest as stagnant density regions in both the isothermal and non isothermal experiments. Kinetic analysis of the data reveals very low activation energies for sintering suggesting that particle rearrangement and agglomeration at low temperatures may be brought about by surface diffusion leading to neck growth and grain rotation. At higher temperatures rapid grain boundary diffusion by overheating along inter particle boundaries induced by sparking may be a dominant sintering mechanism. Although grain growth and densification in conventional WC powders generally obey an inverse relation to each other, in *n*-WC powders both can act synergistically to increase the net densification rate. In fact, complete densification cannot be achieved in *n*-WC powders *without* grain growth as one abets the other.

Keywords: Tungsten carbide; Nano particles; Sintering; Agglomeration

1. Introduction

Consolidation of *n*-WC by solid state sintering methods has developed into a rigorous area of hard carbide research particularly owing to the industrial importance of WC as a very suitable candidate for mechanically arduous environments [1–3]. The low temperatures of solid state sintering enable binderless *n*-WC to be compacted to full density without significant increase in the grain size.

Conventional sintering of micron sized powders is generally considered to be a three stage process. However, various studies suggest that the sintering mechanisms, sintering rate and the activation energies associated with ultra-fine grained powders are considerably different from their micron sized counterparts [4,5]. A general rule seems to be that the more dispersed the initial particles are, the better uniformity and control one achieves over the final grain size. This has led to the current spate of interest in colloidal processing of powders [6,7]. Another particularly interesting feature associated with the sintering of nano sized powders is that they can be sintered at much lower temperatures [5,8,9]. Such characteristics point towards a lowering of the sintering activation energy with a corresponding reduction in particle size. Although the origins of such scaling effects are not clearly known and seem to vary with different systems, it is worth analyzing in detail since it addresses two central issues of engineering importance: the effect of binders/grain growth inhibitors and the effect of initial particle size (and hence green density) in the sintering of WC. Low weight fractions of grain growth inhibitors (NbC, Cr, VC, etc.) are usually incorporated to retard coarsening in *n*-WC [10,11]. Descriptions based on atomistic calculations have provided satisfactory theoretical evidence on the role of such elements [12–14]. But it is still not clear how such nano scale processes translate macroscopically and can be distinguished in a practical sintering experiment. Secondly, agglomerates and fine particles (both of which characterize a green compacted nano powder) sinter differently due to their differences in the pore co-ordination number. Hence it is logical to assume that besides grain coarsening, the competing factors of pore morphology, size distribution, and pore stability are central

* Corresponding author.
E-mail address: aknk27@yahoo.com (A.K.N. Kumar).

0272-8842/$36.00
doi:10.1016/j.ceramint.2011.04.011

issues in controlling the sintering behavior of ultra fine grained WC powders. Combined kinetic and microstructural analyses can clarify these issues and forms the motivation for this work. Our primary objectives were: (i) distinguish the different sintering stages using isothermal and non isothermal sintering data and (ii) identify the sintering mechanisms operative at different temperatures.

2. Experimental

Commercially purchased *n*-WC powder without any pre-treatment with particle sizes measuring ~70 nm (by BET analysis) was used for the experiments. Graphite sheets were used as spacers to separate the powder from the carbon die and punch. Spark plasma sintering (SPS), which is an effective method to compact *n*-WC without much grain growth was used to consolidate the powders (Dr Sinter Lab). The instrument has a dilatometer with an accuracy of 0.01 mm that was used for measuring the instantaneous linear shrinkage. Temperature measurements were carried out using a radiation thermometer (pyrometer) that was focused on a small hole in the graphite die. An initial temperature ramp until 873 K followed by a pre-sintering isothermal hold for temperature stabilization was carried out at 873 K for 3 min. The actual sintering experiment was carried out in vacuum (<4 Pa) at a constant heating rate of 50 K/min and a pressure of 50 MPa to various temperatures: from 1073 K to 1873 K. The samples were held at these temperatures for a period of 20–35 min during which time their shrinkage was continuously monitored using the dilatometer. Longer hold times resulted in oxidation of the samples and hence were avoided. The non isothermal, constant heating rate (CRH) experiments were conducted under similar conditions, but at two different heating rates of 20 and 50 K/min with the temperature increased continuously until shrinkage change reduced to zero. For density measurements, the samples were polished and the displacement (Archimedes) method was used. Grain sizes were measured on fractured specimens using a FE SEM. Approximately 100 grains were sampled and the average values are shown. Before discussing the results, we first provide a brief overview of the kinetic equations used to analyse the data.

3. Kinetic equations applied to the sintering theory

For the non isothermal (CRH) technique, the model of Young and Cutler [15] was utilized to understand the sintering behavior in which GB and lattice controlled sintering can be identified and effective activation energies mQ (where $m = 1/2$ for lattice diffusion and 1/3 for GB diffusion) can be determined from the slopes of $\ln(Td\varepsilon/dT)$ vs. $1/T$ graphs. Although other sintering mechanisms are difficult to identify, the primary advantage of CRH experiments is that a single experiment can provide a general idea of the entire process. However, unless either m or Q is known beforehand, the individual mechanisms cannot be quantitatively distinguished and only the effective activation energy, mQ can be determined from the relevant plots. To determine m, the isothermal technique was adopted.

Generally, the isothermal sintering kinetics (either solid or liquid phase assisted) during initial stage sintering can be described by an equation of the type:

$$\varepsilon^m = \left(\frac{\Delta l}{l_0}\right)^m = \frac{Kt}{TG^n} \tag{1}$$

where 'm' is the sintering exponent, t is the isothermal holding time, G is the particle size, 'n' is the grain growth or coarsening exponent and T is the hold temperature. The form of K can be related to temperature by an Arrhenius type equation, $K = K_0 \exp(-Q/RT)$, where Q refers to the activation energy for densification and R is the gas constant. The kinetic parameters can be evaluated easily by a simple modification of the sintering equation as follows:

$$\ln \varepsilon = \frac{1}{m}\ln\left(\frac{K}{Td}\right) + \frac{1}{m}\ln t \tag{2}$$

Therefore a plot of $\ln(\varepsilon)$ against $\ln(t)$ should give a straight line with slope $1/m$ provided there is no grain growth ($G^n = d = \text{const}$). The general form of this equation (plot of $\ln(\varepsilon)$ against $\ln(t)$) has been frequently employed to describe the isothermal sintering of nano powders at various temperatures and relative densities [16]. The commonly employed models of Kingery [17] and Coble [18] predict m to be either 1.5 (lattice diffusion (LD) through defects), 2 (grain boundary (GB) recreation), 2.5 (pure LD) or 3 (GB diffusion).

When neck formation is succeeded by interconnected pore structures, the intermediate stage is said to have started. We used the tetrakaidecahedron model of Coble [19,20] to analyse the data. The relevant shrinkage kinetics is derived in terms of porosity (pore fraction) rather than linear shrinkage and assuming a cylindrical pore as:

(a) Lattice diffusion without grain growth

$$P - P_0 = \frac{N_A D_v \Omega \gamma}{k_B T G^3} t \tag{3}$$

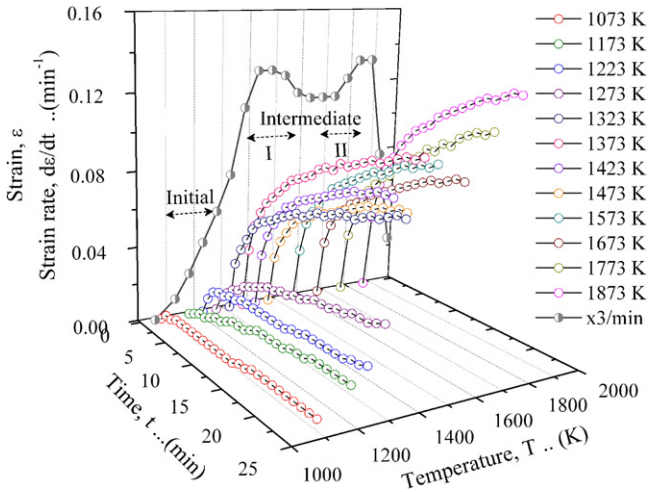

Fig. 1. Combined isothermal–CRH sintering curves.

(b) Lattice diffusion with grain growth

$$P - P_0 = \frac{N_A D_v \Omega \gamma}{k_B T} \ln t \quad (4)$$

(c) Grain boundary diffusion without grain growth

$$P - P_0 = \left(\frac{N_A D_b w \Omega \gamma}{k_B T G^4} \right)^{2/3} t^{2/3} \quad (5)$$

where the terms have the following meanings: P_0 – initial porosity at $t = 0$ in the intermediate stage, P – final porosity, D_v, D_b – volume, grain boundary diffusivities, γ – surface energy, w – grain boundary width, Ω – atomic volume and the other terms have their usual meanings. Hence a plot of $(P–P_0)$ against t^m or $\ln(t)$ should give a straight line from which the primary sintering mechanism can be deduced based on the value of m ($m = 1$ or 0.667 for lattice or GB diffusion as may be the case discussed above). For cases in which there is concurrent grain growth, a diffusion limited growth with $d \propto t^{1/3}$ was considered by Coble in the above equations. Activation energies from the isothermal experiments were calculated using Dorn's method [21]:

$$\frac{d\varepsilon}{dt} = Ke^{-(Q/RT)}t \quad (6)$$

Here, the densification strain rates were evaluated at a constant time at different sintering temperatures so that a plot of $\ln(d\varepsilon/dt)$

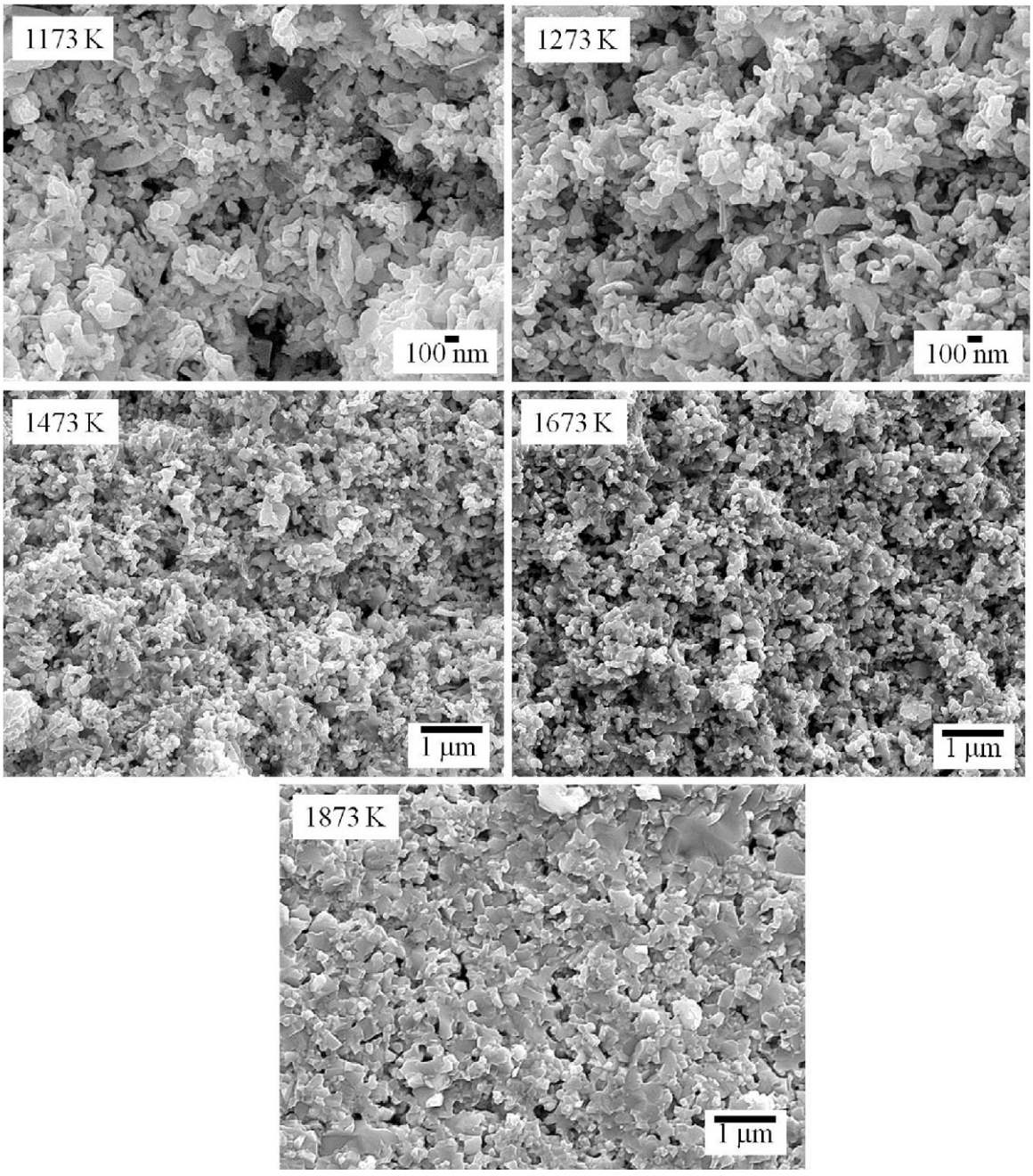

Fig. 2. Microstructures of the samples interrupted at various temperatures.

against $1/T$ would yield values of Q. Usually the Dorn method is associated with an error of ~8 to 10%.

Identifying an individual sintering stage (initial neck formation and growth) in such nano-scale compacts by microstructural observations alone is tedious. Moreover, a large fraction of the net sintering strain occurs during heat-up of the samples and hence the initial stages can be completely overshadowed by the time the higher sintering temperatures are reached. To overcome this difficulty, the CRH curves (at fast and slow heating rates) were first checked for variation in sintering strain rates. This was then compared with the isothermal sintering strain curves. Fig. 1 shows the combined CRH-Iso sinter curves which clearly follow each other. Slope changes in any temperature range in the CRH experiments were taken to represent a change in sintering mechanism from the previous stage and isothermal kinetic analyses were also conducted similarly. Initial stage kinetic equations were applied at those temperatures where the net isothermal sintering strains were less than 5%. This seemed to be a logical method to isolate sintering stages without compromising too much on overlap of sintering mechanisms. Further, the samples were also observed by high resolution FE SEM to check their microstructure. In the following sections we first present the results of the isothermal and CRH experiments and the kinetic data analyses.

4. Results

4.1. Microstructure

A few representative microstructures at different stages of the sintering process are shown in Fig. 2. From 1173 K to 1323 K, the individual particles and bonded particles with necking can be discerned as a dispersed phase indicating the initial sintering stage. A few agglomerates can also be seen. From around 1373 K to 1773 K, large continuous pores can be clearly discerned and were taken to represent the intermediate stage of sintering. At 1873 K, most of the pore phase is pinched off, leading to the final sintering stage. However, the actual transition from the initial to intermediate stage sintering is rather vague as there are strong density gradients in the microstructure due to agglomeration. But as a preliminary estimate, micrographs from these temperature ranges combined with the CRH-Iso sinter curves mentioned earlier can be assumed to represent the different sintering stages.

4.2. Isothermal sintering

Fig. 3a and b shows the shrinkage strain data along with the linear fits using Eq. (2) in the first stage covering 1073–1273 K. The total shrinkage is less than 5% but the sintering exponent varies between 1.46 (lattice diffusion controlled by movement through defects) at 1173 K and 2.14 (GB diffusion) at 1273 K and no consistency in values could be obtained at the other temperatures. However, looking at the sintering strain curves (Fig. 3a), it seems that at 1073 K, there is almost no densification for longer holding times implying that a non densifying mechanism of neck growth is operative. Secondly, at

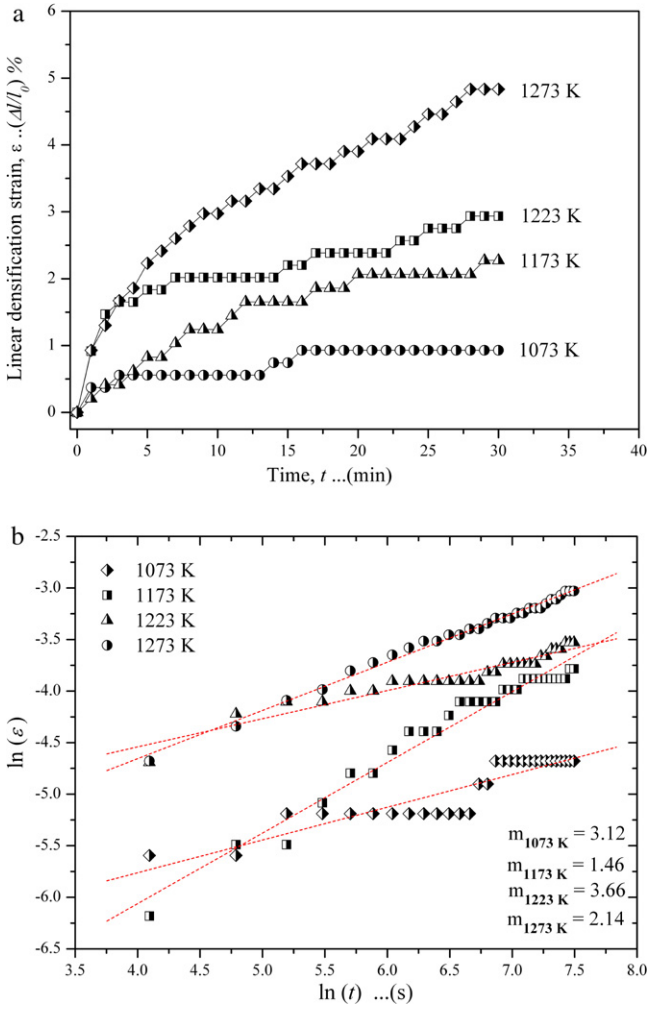

Fig. 3. (a) Shrinkage strain and (b) plot of ln(ε) vs. ln(t) from 1073 K to 1273 K.

all these temperatures, the samples reach an end point density implying that isothermal sintering at these temperatures is futile. At higher temperatures, towards the end of the initial stage ($T > 1273$ K), the isothermal sintering strains increase. Generally, the sintering mechanism seems to alter in this narrow temperature range such that at $T \leq 1073$ K, densification is retarded and as the temperature increases, shrinkage also increases initially by LD through defects and later by recreation of grain boundaries. Irrespective of the sintering mechanism, the initial temperature range shows two characteristics: presence of a strong non densifying mechanism and end point densities.

For analyzing the intermediate stage, the porosity fraction was estimated as $P = 1 - \rho$, where $\rho = (1 - \varepsilon)^3$ ρ_f is the instantaneous density and ρ_f is the final density expressed as a fraction of the theoretical density. Fig. 4 shows the porosity and relative densities of the samples at different temperatures in the intermediate stage. At the start of the isothermal hold period, the porosity was ~35 to 42% (at various temperatures) which decreases to anywhere between 6 and 18% at the end of the hold period. It is interesting to note that although the density (porosity) increases (decreases) with the hold time, they are almost constant in a narrow range of temperature (~1400 to

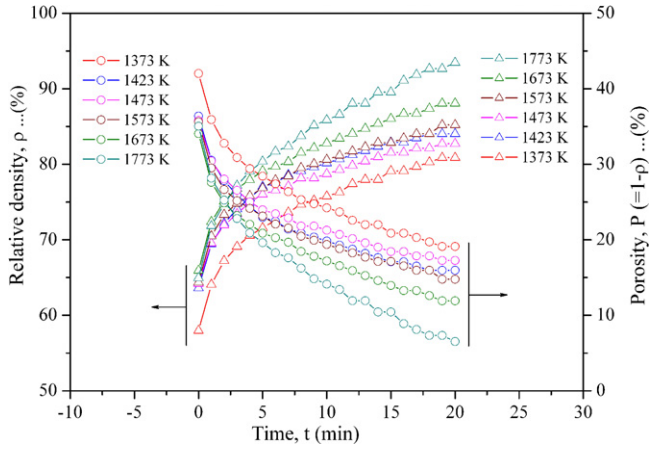

Fig. 4. Relative density and porosity during isothermal hold at various temperatures.

1573 K). The end density (porosity) seems to be a strong function of the initial density (porosity) at $t = 0$.

The sintering kinetics was analyzed by plotting the incremental porosity $P - P_0$, against t^m (Fig. 5a and b). In the temperature range 1373–1773 K, the data points fall in a straight line with $m = 0.66$, suggestive of Coble's analysis of GB diffusion with no grain growth (Eq. (5)). However, at higher temperatures (1573–1773 K), the slope of the lines changed distinctly. This could be due to grain growth and faceting in the system. Coble's theory for GB diffusion discussed in the earlier section does not consider simultaneous coarsening. But we measured the actual grain sizes during isothermal hold at 1773 K and indeed found a relation of the form $G^2 = G_0^2 + At$. This type of interface controlled growth kinetics (growth exponent = 2) in *n*-WC has been confirmed earlier [22]. Moreover, for long hold periods, the fraction of faceted grains also increased as grain growth proceeds by coalescence. At 1873 K, the data did not satisfactorily fit the proposed GB diffusion model probably due to the changeover from continuous to isolated porosity (final stage sintering). However, non availability of data at higher temperatures precluded any further analysis of the sintering mechanism at this temperature. Moreover, for all these data plots, the initial few minutes show a change in slope. The effect is magnified in the initial temperature range than in the latter. This could either mean a changeover in the actual mechanism by a change in pore morphology/initial stage sintering or else an instrumental fluctuation. Due to the sufficiently fast heating rate (50 K/min) employed, we believe that the sample would require a few minutes at the hold temperature for stabilization so as to achieve a uniform temperature distribution throughout the sample. To check this, a set of samples were interrupted at different times of isothermal hold (t = 1, 6, 12 and 20 min) and the actual densities were measured. This was then compared with the calculated instantaneous density values. Only after the initial 2–3 min did the measured and calculated values converge (figure not shown). Based on this reasoning, the non linearity in the data during the first few minutes was therefore neglected.

The apparent activation energy of sintering was calculated using the Dorn method. Only positive values of slope were considered. In the designated initial stage from 1173 K to ~1323 K (Fig. 6), Q = 111 kJ/mol. In the final stages (1673–1823 K), a small activation energy of 45 kJ/mol was determined (figure not shown). The other temperature ranges

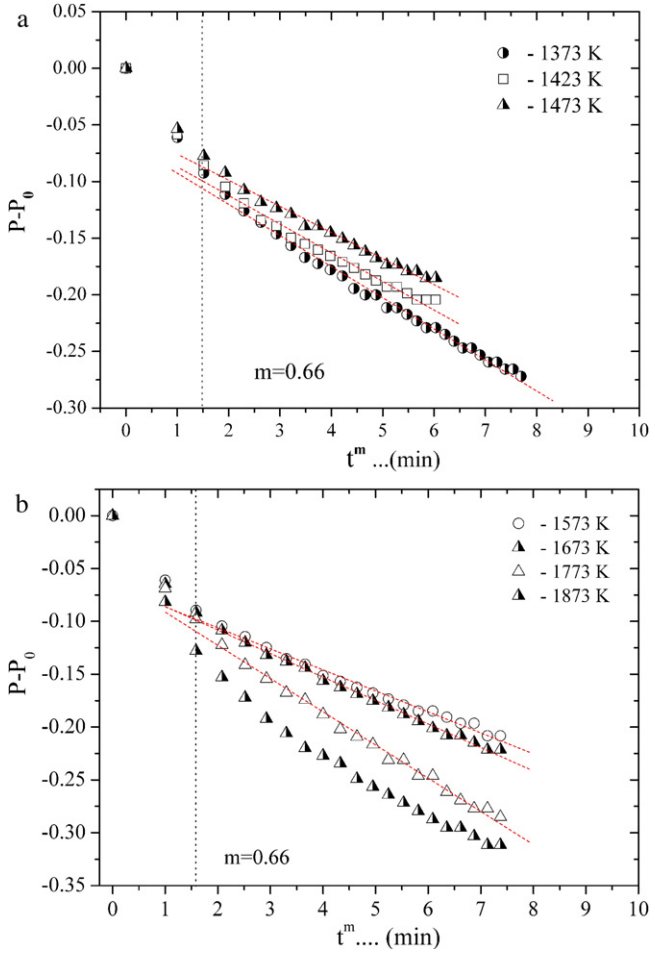

Fig. 5. Sintering kinetics of intermediate stage at (a) 1373–1473 K and (b) 1573–1873 K.

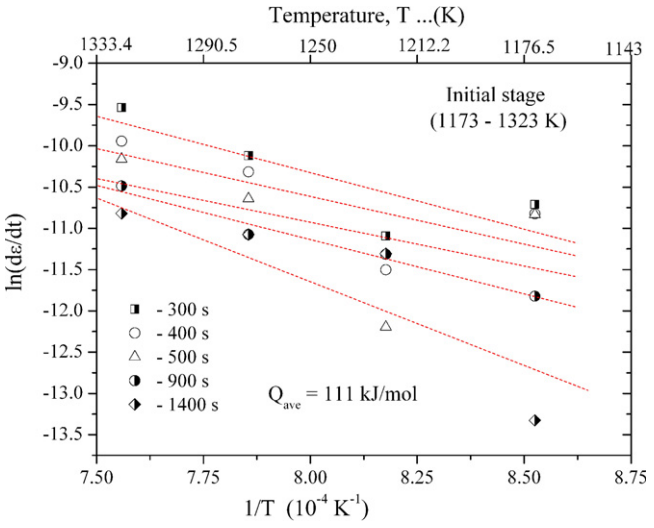

Fig. 6. Activation energy calculated by Dorn method.

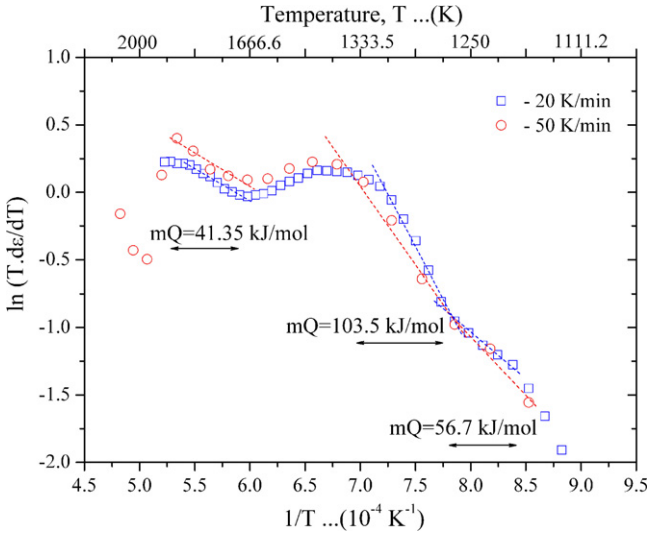

Fig. 7. Effective activation energies calculated by Young and Cutler's method.

could not be analyzed without ambiguity since sintering strains between the temperatures varied rapidly and our sampling interval (every 50 or 100 K) was inadequate to collect sufficient data points. The CRH experiments were hence considered for analysis at higher temperatures.

4.3. Non isothermal (CRH) sintering

Fig. 7 shows a plot of $\ln(T d\varepsilon/dT)$ vs. $1/T$ for the CRH experiments along with the measured values of the effective activation energy. Low heating rates were found to show transition stages clearly. Three different sintering stages can be identified from 1173 K to 1873 K by the change in slope: a first stage ranging from 1173 to 1273 K with $mQ = 56.7$ kJ/mol, a second stage from 1323 to 1473 K and $mQ = 103.5$ kJ/mol and a third stage with $mQ = 41.35$ kJ/mol between 1673 and 1823 K. Consistent with the results of the Dorn method shown earlier, in the CRH experiments also between the second and third regions, there was a narrow range with negative slope. The activation energy for sintering controlled by lattice diffusion ($m = 1/2$) in the I stage is $Q_I = 113.4$ kJ/mol which agrees very well with the calculations of the Dorn method for isothermal sintering ($Q_I = 111$ kJ/mol). In the second stage, assuming GB diffusion ($m = 1/3$), $Q_{II} = 310.5$ kJ/mol which closely corresponds to the activation energy for GB diffusion of C in WC [23]. The third stage shows a low activation energy, which could not be correlated to any reported solid state diffusion mechanism.

5. Discussion

5.1. Diffusion mechanism and activation energies

In compound systems, sintering is generally considered to occur by the slowest species diffusing through the fastest route. Buhsmer and Crayton [23] studied the diffusion of tracer Carbon (^{14}C) in WC by layer growth and concluded that diffusion occurred initially by LD and later on by GB diffusion through the WC grains. The LD coefficient was very low compared to the GB diffusion with the diffusivity ratio, D_{gb}/D_v being 10^3 ($D_{gb} \approx 10^{-5}$ cm^2/s at 2238 K). The activation energy for grain boundary diffusion of ^{14}C was estimated to be ≈300 kJ/mol. Activation energy for W diffusion in WC is still higher (the diffusion coefficient being orders of magnitude lower than that of C). Yet, very low activation energies comparable to our present results during the initial stage have been consistently reported although no single mechanism has been confirmed (see Table 1 for comparison). Going by these data, it is clear that sintering in *n*-WC is greatly enhanced. Studies on necking of WC spheres during initial stage suggest volume and surface diffusion to be the dominant sintering mechanisms while there are also speculations that the intermediate stage may be a two-step process [24]. The analysis from diffusion experiments and the recent emerging reports from sintering analysis strongly point to three major factors that enhance sintering in WC: particle size, activation by external fields and fine microstructure.

Low activation energies of the order of 110 kJ/mol cannot be associated with any known mass transport mechanism in WC. However sintering activation energies can be substantially lowered when surface diffusion (SD) occurs in addition to LD such that both densification and neck growth (by SD) occur

Table 1
Comparison of sintering parameters calculated from isothermal and CRH experiments.

Sintering method (particle size)	Temperature (K)	Q (kJ/mol)	Sintering mechanism	Ref.
Isothermal sintering				
Conventional (100–500 nm)	1223–1523	76	Neck formation	[24]
Microwave (128 μm)	1173–1223	69	SD (neck growth) and LD (densification)	[25]
	1473–1673	–	SD (neck growth only)	
SPS (70–100 nm)	1173–1323	111	SD, LD via defects	Present
	1373–1573	–	GB diffusion	Present
	>1573	45	GB diffusion (with grain growth)	Present

Sintering stage	Temperature (K)	mQ (kJ/mol)	Possible mechanism
Non isothermal sintering (CRH) – (present work)			
I	1173–1273	56.7	Lattice diffusion (defects)
II	1323–1473	103.5	GB diffusion
III	1623–1773	41.35	–

simultaneously. At low temperatures ($T \leq 1073$ K), shrinkage strains are substantially low (<1%) indicating that the primary sintering mechanism is non densifying. Between 1073 K and 1273 K, the shrinkage strains increase owing to increased contribution by defect assisted LD along with SD. Correlation with calculated activation energies seems to suggest that sintering in this temperature range may occur primarily by diffusion of C through the lattice defects. However, end point density phenomenon is also observed in the low temperature range (around 1073 K) which cannot be explained if LD (through defects) alone was the chief densifying mechanism. Particle rearrangement (PR) is a possible mechanism that can explain the observed behavior. PR usually occurs at low temperatures, starts with a minor shrinkage and leads to an end point density when the closest packing is reached. Hence, sintering by PR leads to significant shrinkage during the early stages of heating and can be enhanced in nano particles due to combined SD and defect-assisted LD. The low sintering activation energy observed during the initial stage may therefore be attributed to a densification mechanism brought about by a combination of LD through defects and PR assisted by SD.

Secondly, the process of activated sintering by SPS is assumed to generate sparks between particles. This results in overheating at inter-particle boundaries such that an overshoot to the melting point can be expected at particle surfaces leading to localized melting. Like conventional liquid phase sintering, the presence of an ultra thin liquid layer at the inter-particle boundaries can lead to swift diffusion and rapid neck growth with low activation energies. This also enhances grain rotation and PR. With increase in the average temperature, the current pulse also increases proportionally (600–700 A at peak in the present experiments with 12 s on time and 2 s off time) so that the sparking phenomenon increases with sintering temperature. Such a large current density between small particles leads to arcing and formation of a surface liquid layer. When substantial grain growth has already occurred, the GB and inter-particle boundary are synonymous and readily form the preferred route for mass transport during sintering.

Finally, nano powders are generally associated with agglomeration in which groups of small particles demarcated by GBs coalesce to form larger aggregates with pore boundaries. This results in a totally non uniform microstructure and may lead to non uniform densification (as discussed in the next sections) and multiple routes to sintering. Hence, the concept of the fastest diffusion route during sintering becomes complicated as intra agglomerate pores may densify by GB diffusion while the larger pores may require higher energies for densification.

Nevertheless, the low activation energies in *n*-WC seem to suggest that both the W and C atoms diffuse quickly during sintering by short range diffusion. The general mechanism

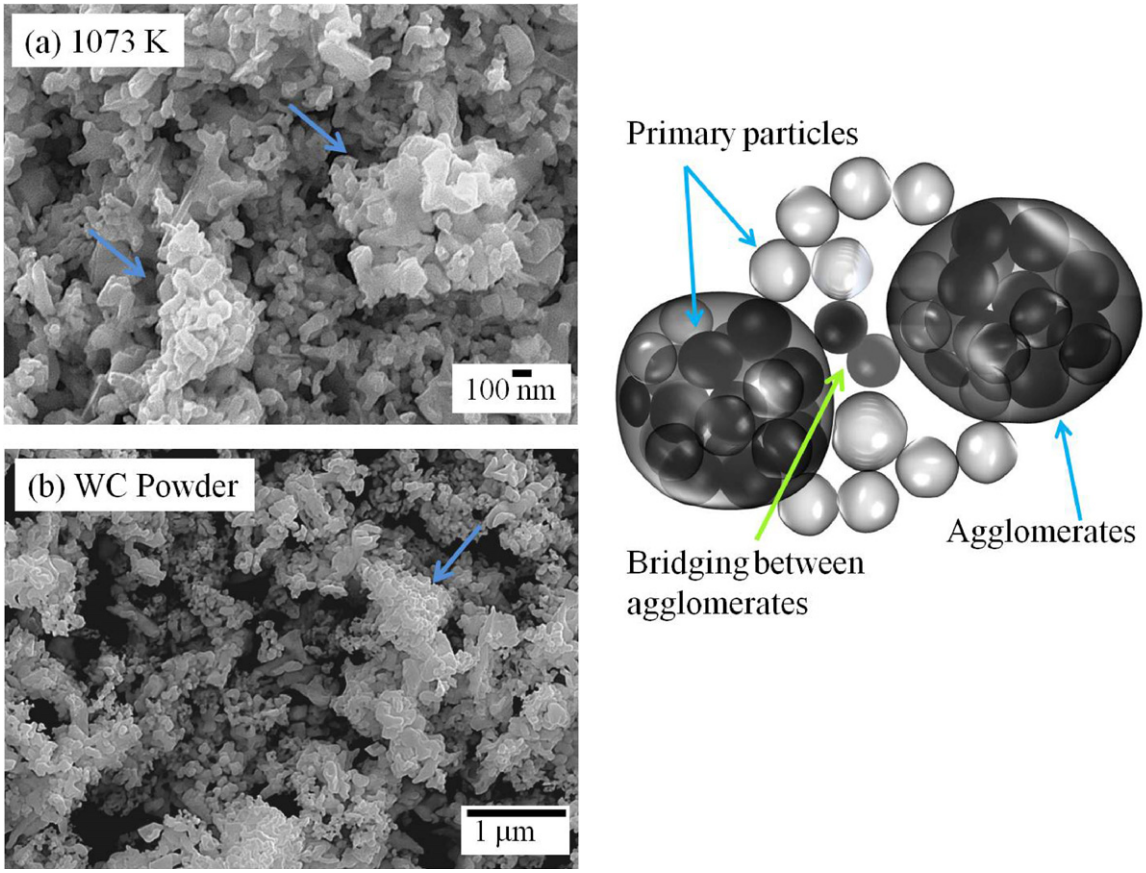

Fig. 8. (a) Image of compact interrupted at 1073 K with arrows indicating agglomerates and (right) schematic of the microstructure. (b) SEM image of *n*-WC powder indicating presence of agglomerates.

seems to be strongly controlled by SD at low temperatures with a small component of densification arising by LD through defects/PR and at high temperatures by GB diffusion. The inadequacies notwithstanding, both the isothermal and CRH experiments strongly indicate the occurrence of sub-stages in the sintering process. In the later stages, the Q values determined by either technique are not similar. We attribute this discrepancy to a finite change in microstructure brought about by either a change in particle shape, size or pore geometry which is not accounted for by both the theories.

5.2. Sintering mechanisms

The combined isothermal and CRH sintering data (Fig. 1) clearly show that the isothermal strain has a peak sintering at two temperatures: around 1373 K and 1873 K. This corresponds to the maximum in the strain-rate curve which represents the CRH experiment. Following this, both CRH and isothermal sintering strains decrease and increase until the final stage is reached. Observations of microstructure at the intermediate temperatures help to explain the sintering behavior and evolution of the sintering strain curves.

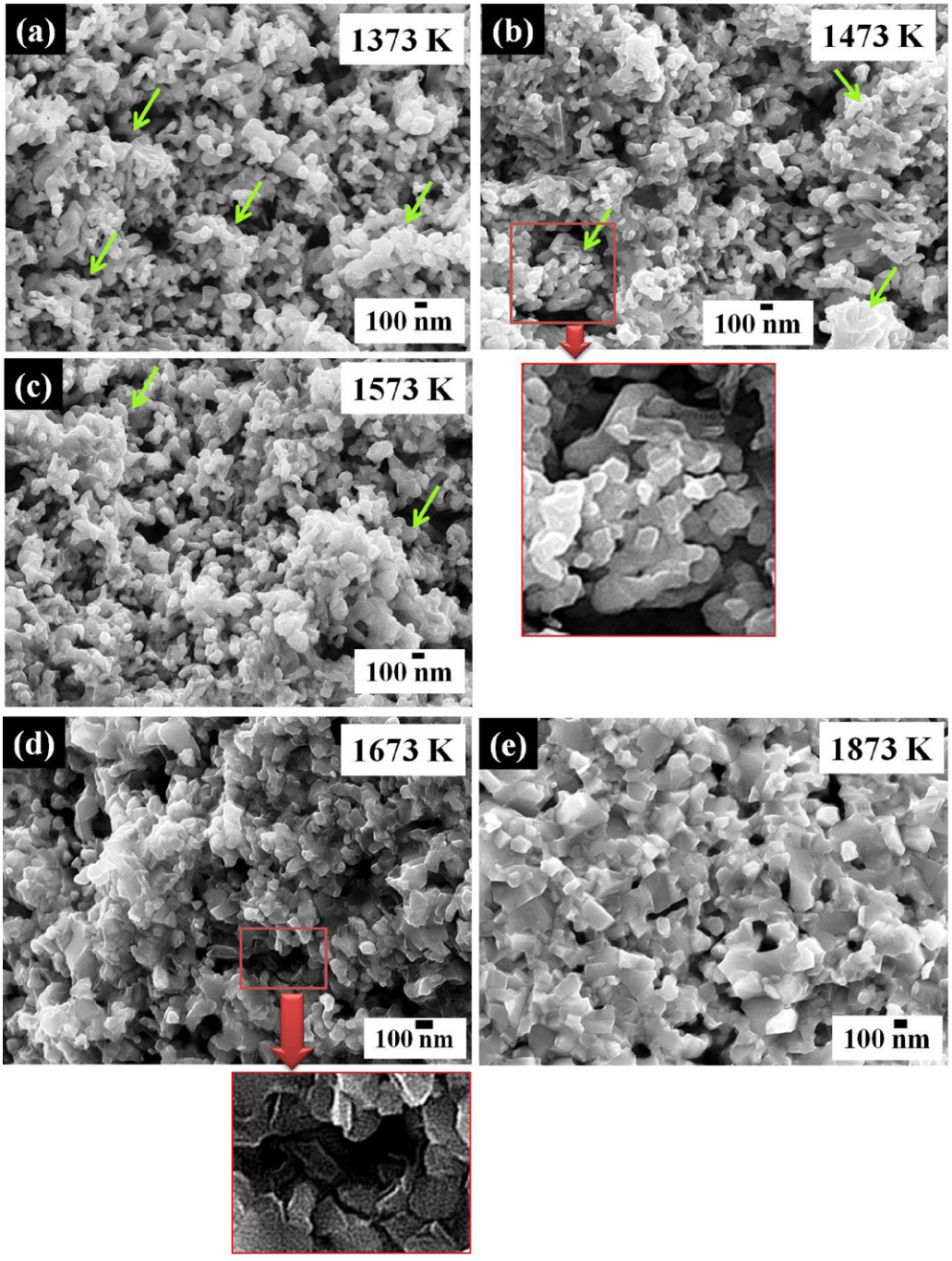

Fig. 9. Microstructures at various sintering temperatures along with magnified images of certain regions. Arrows indicate agglomerates.

Fig. 8 shows a high magnification view and schematic of the microstructure of a compact interrupted at 1073 K and also the initial powder, which shows a composite phase consisting of both individual particles and clusters of connected particles that have undergone necking. The clusters are hard agglomerates that persist even after application of the external pressure. Presence of such agglomerates in the powders can affect the green density of the samples and accordingly in all the samples studied, the green density was less than 43%. It is evident that even at low temperatures the inter particle necking has occurred. In the initial stages of sintering, hard particles like WC usually undergo particle rearrangement and plastic deformation at slightly higher temperatures and pressure that can lead to defect generation in the lattice [26]. The question of plastic deformation can be addressed by looking at the Hertzian contact stresses during initial stages of contact between the particles. Contact stresses assume significance in pressed nano particles particularly in the initial stage sintering because the applied external pressure acts over a very small contact area which induces an associated stress that is very large leading to instantaneous plastic flow. The maximum contact pressure (Hertz stress) is given by [27]:

$$P_0 = \frac{1}{\pi}\left(\frac{6PE^{*2}}{R^2}\right)^{1/3} \tag{7}$$

where P is the applied force, which for the experimentally applied pressure of 50 MPa over a 10 mm diameter cylindrical graphite die corresponds to ≈4 kN, $1/R = (1/R_1 + 1/R_2)$ is the effective curvature of particles of radii R_1 and R_2 (≈70 nm) and $E^* = E/(1 - \nu^2)$ is the reduced or contact modulus with ν (≈0.3) and E (≈550 GPa) being the Poisson ratio and elastic modulus of WC, respectively. The mean contact pressure is then given by $\overline{P} = 0.66P_0$ which turns out to ≈40×10^3 GPa. This can be considered to be the maximum stress acting between any two particles in the green compact. Hence, in addition to curvature-induced atom transport, such a large magnitude of stress drives instantaneous plastic flow so as to increase the contact area resulting in immediate necking.

Fig. 9(a–c) shows the high magnification microstructure of the samples from 1373 K to 1573 K. The agglomerates are enhanced and importantly, two different types of pore morphologies can be clearly distinguished: long, continuous inter-agglomerate pores and small disconnected intra-agglomerate pores (inter-particle pores). With increase in temperature, the individual agglomerates densify by sintering and slight grain growth, while there is not much observable change in the nature of the inter-agglomerate pores. The earlier kinetic data analysis suggests that the sintering in this range is controlled by grain boundary diffusion. At 1673 K, the grains can be clearly discerned and the intra-agglomerate pores have mostly vanished, replaced by only continuous pores (Fig. 9d). At still higher temperatures, (1873 K), the continuous pores become isolated and pinched-off resembling the final sintering stage (Fig. 9e).

It is clear that the intermediate stage is governed by agglomerate evolution. When agglomerates form, internal density gradients are set up leading to a large pore size distribution. Consequently, sintering sub-stages are introduced in the intermediate stage by the differences in the sintering kinetics of the inter and intra agglomerate pores. On observation, four important stages can be visualized (Fig. 10):

5.2.1. Stage I (∼80% end density)

This corresponds to the end of the initial stage/beginning of the intermediate stage and covering the temperature range ∼1300 to 1400 K. In this stage, there is a rapid increase in the densification rate of the compact. The shrinkage has two components: one arising from inter agglomerate and another from intra agglomerate densification. The end densities increase to around 80% from an initial density of 57–65%. At the end of this stage, most of the bridges between agglomerates disappear, the clusters impinge upon each other and a microstructure characterized largely by agglomerate and continuous pore distribution is reached.

5.2.2. Stage II (∼83 to 85% end density)

The initial rapid shrinkage is followed by an almost constant density regime characterized by the clusters shrinking in upon themselves. The shrinkage of the compact, if any, occurs purely by intra agglomerate densification. As Lange [28] has pointed out, this is equivalent to a net compressive stress acting on each agglomerate and the rate at which they shrink is proportional to the number of necks in the intra agglomerate phase. However, when the original agglomerates are dense (as in the present case), there is not much increase in densification. Hence, the shrinkage caused by sintering of micro pores within the agglomerates is not large enough to warrant any perceptible change in the macroscopic shrinkage strain rate. Over the range of temperatures where such behavior is exhibited, the net density increase should remain constant. However, due to the breakage of inter agglomerate bonds, the sintering strain rate and isothermal sintering strain also decrease. This results in a small decrease in relative density of about 2–3% from that of lower temperatures. The microstructure evolves into well-demarcated agglomerate boundaries.

5.2.3. Stage III (∼85% end density)

Following the formation of stable agglomerates, intra agglomerate shrinkage cannot proceed further although sintering by grain growth occurs to a small extent. From this point, the sinterability of inter agglomerate pores controls the densification rate. But this is also prevented because of the large pore co-ordination number N. The dihedral angle (ψ) in WC–Co is reported to vary between 30 and 120° [29]. Although WC crystals have a strong tendency for faceting and these values are strongly dependant on the contacting facets, as an approximation, the statistical average of 75° can be used. The critical pore co-ordination number, N_c can then be calculated from [26]:

$$N_c = \frac{360}{180 - \psi} \tag{8}$$

In this case, with $\psi \approx 75°$, N_c ∼3.5. From the microstructure it is clear that many of the large pores are surrounded by more

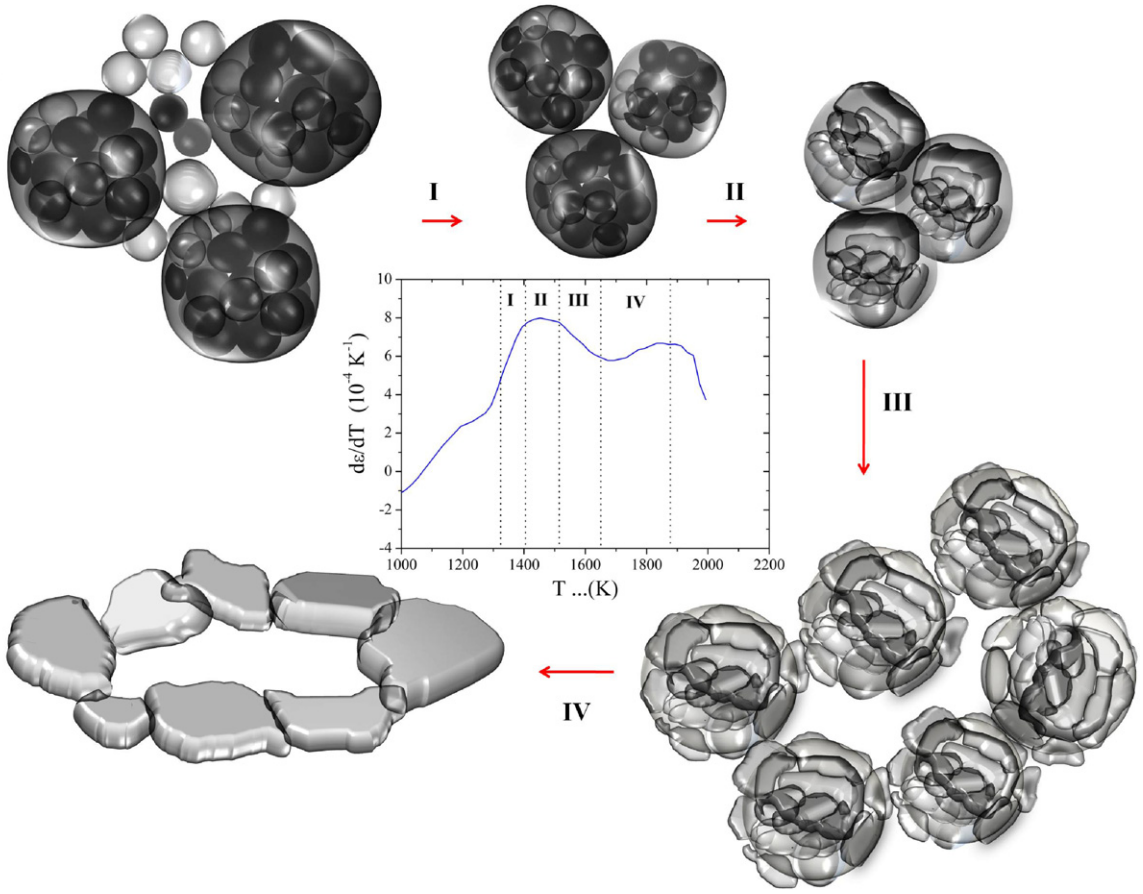

Fig. 10. Schematic of the sintering mechanism of *n*-WC on the basis of the experimental shrinkage strain rate in a CRH experiment.

than the critical number of grains. This inter-agglomerate pore stability retards the shrinkage rate as observed in the intermediate stage. The net shrinkage strain rate decreases due to two simultaneous forces opposing densification: large co-ordination number and a small amount of grain growth within the agglomerates. The relative density also decreases further since the large pores start to grow.

5.2.4. Stage IV (~94% end density)

Following the small dip in shrinkage strain rate, there is a passive period over which the system tries to evolve by massive particle growth *within* the agglomerates. This occurs not only as a result of temperature driven growth but also to reduce the pore co-ordination number. The massive grain growth leads to a breakup of the agglomerate identity into large grains and the stable inter agglomerate pores now start to sinter. These simultaneous processes of massive grain growth and pore shrinkage balance each other initially. As the agglomerates continuously convert into large grains, the pores start to shrink rapidly, surpassing the grain growth rate. Hence concurrent grain growth supports shrinkage until the continuous pores are eliminated and the isolated pore structure resembling the final stage appears. The relative densities increase to nearly 94% during this stage. The final stage sintering is reached at temperatures above 1773 K when the pore phases are pinched off which again results in a reduction of the densification rate.

The sintering of *n*-WC thus seems to be integrated with three controlling factors: initial density, grain size and pore co-ordination number at any instant. Fig. 11 shows the dependence of densification behavior on the grain size and measured bulk density. It is clear that there is a narrow region in the intermediate stage where the relative density stagnates (increases and decreases marginally at ~85%) after which it

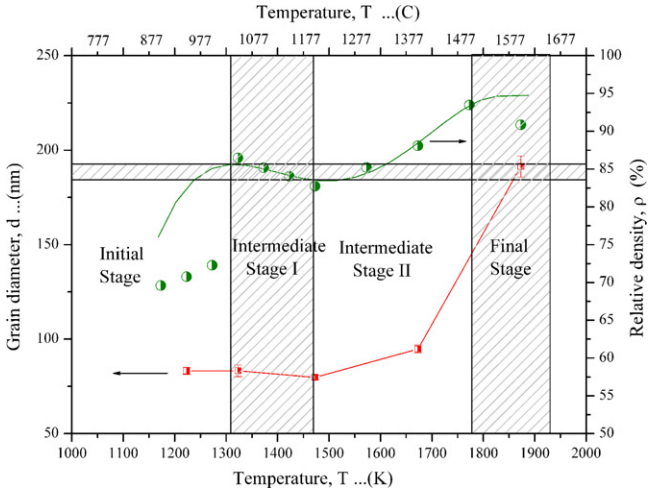

Fig. 11. Dependence of grain size, bulk density and temperature on the sintering stages in *n*-WC.

increases steadily. The sporadic variation in density is brought about by mechanisms controlling agglomerate evolution. Isothermal sintering at these constant density regions cannot yield a dense compact. Grain growth within agglomerates is hence a necessary step for complete sintering.

In the light of the present results, a few points are worth discussing in further detail: first, it is clear that a heterogeneous packing, low green density and agglomeration can readily lead to a multi-staged sintering process. The sintering of such composite microstructures is controlled by the sinterability of the pores. Nano scaled powders usually have a tendency to form agglomerates that sinter by the mechanism detailed in this study. Pre-sintering processes like ball milling of the ultra fine powder with binders usually produces agglomerates which lead to grain growth and multi stage sintering. An increase in the pressure on the green compact does not necessarily imply low agglomeration, particularly when the agglomerates are composed of hard particles. Instead, the intra-agglomerate particles undergo necking, rearrangement and sintering without altering the general inter-agglomerate geometry. This might alter the peak densification temperature of the compact although the sintering mechanism may be expected to generally remain the same. Secondly, the presence of agglomerates also necessitates the requirement of an increase in temperature for any further increase in densification. Hence, the isothermal sintering almost always reaches an end-point density because the inter-agglomerate pores effectively retard densification unless the temperature is increased. As Kellett and Lange [30] have pointed out, for a fixed sintering temperature and time, the end point density is proportional to the bulk density of the powder. Unless the microstructure evolves by an increase in temperature to reach a stage where the agglomerates are replaced by well-formed grains and inter-granular porosity, an end point density will always be observed. Thirdly, arcing between particles in the agglomerate during SPS might accelerate the agglomerate densification process and reduce the sintering temperature. This is advantageous to restrict grain growth at higher temperatures while still achieving densification and may prove to be a major cause for the low sintering temperatures consistently observed when using this method for sintering *n*-WC. Nevertheless, a minimum amount of grain growth is imperative to cross the sintering barrier presented by the inter agglomerate pores. An agglomerate-free ultra fine grained powder may thus prove to be a better choice for obtaining a dense, nano grained WC compact.

6. Conclusion

The sintering of *n*-WC powders is observed to be a multi staged process in which agglomerates play a major role in controlling the densification kinetics. Although LD through defects and particle rearrangement assisted by SD were found to control low temperature sintering, the isothermal and non isothermal kinetics evaluated at various higher temperatures suggest that sintering occurs by GB diffusion with simultaneous grain growth for a large part of the compaction process. The presence of agglomerates introduces sub-stages in the sintering process which can effectively decrease the densification rate unless grain growth occurs to overcome the shrinkage barrier. Pre-sintering processes and the presence of binders and grain growth inhibitors can hence play a crucial role if they alter the surface energy or the tendency for agglomeration of the *n*-WC powders.

Acknowledgements

One of the authors, A.K.N.K. wishes to express his gratitude to Prof. K.Kurokawa and Dr. A Yamauchi, Hokkaido University for their hospitality during his stay in Japan and for introducing him to this work. A.K.N.K. also acknowledges a fellowship grant from the Ministry of Education, Culture, Sports, Science and Technology of Japan.

References

[1] L. Bartha, P. Atato, A.L. Toth, R. Porat, S. Berger, A. Rosen, Investigation of hip-sintering of nanocrystalline WC/Co powder, J. Adv. Mater. 32 (2000) 23–26.
[2] D. Agrawal, J. Cheng, P. Seegopaul, L. Gao, Grain growth control in microwave sintering of ultrafine WC–Co composite powder compacts, Powder Metall. 43 (2000) 15–16.
[3] H.C. Kim, D.Y. Oh, I.J. Shon, Sintering of nanophase WC–15 vol.% Co hard metals by rapid sintering process, Int. J. Refract. Met. Hard Mater. 22 (2004) 197–203.
[4] W.D. Schubert, A. Bock, B. Lux, General aspects and limits of conventional ultrafine WC powder manufacture and hard metal production, Int. J. Refract. Met. Hard Mater. 13 (1995) 281–296.
[5] J.R. Groza, R.J. Dowding, Nanoparticulate materials densification, Nanostructured Mater. 7 (1996) 749–768.
[6] A.J. Sanchez, A. Millan, N.I. Nieto, R. Moreno, Aqueous colloidal processing of nickel powders, Acta Mater. 49 (2001) 645–651.
[7] Laarz Eric, Lennart Bergstrom, Dispersing WC–Co powders in aqueous media with polyethylinimine, Int. J. Refract. Met. Hard Mater. 18 (2000) 281–286.
[8] A. Pechenik, G.J. Piermarini, S.C. Danforth, Fabrication of transparent silicon nitride from nano size particles, J. Am. Ceram. Soc. 75 (1992) 3283–3288.
[9] Chang Jia Cheng, Hua Tang, Xue-Zhen Mei, Fa-Zhang Yin, QuF Xuan-Hui, Spark plasma sintering on nanometer scale WC–Co powder, Mater. Lett. 59 (2005) 2566–2569.
[10] Xiao Dai-hong, Yue-hui He, Wei-hong Luo, Min Song, Effect of VC and NbC additions on microstructure and properties of ultrafine WC–10Co cemented carbides, Trans. Nonferrous Met. Soc. China 19 (2009) 1520–1525.
[11] J. Weidow, S. Norgren, H. Andren, Effect of V, Cr and Mn additions on the microstructure of WC–Co, Int. J. Refract. Met. Hard Mater. 27 (2009) 817–822.
[12] Christensen Mikael, Goran Wahnstrom, Effects of cobalt intergranular segregation on interface energetics in WC–Co, Acta Mater. 52 (2004) 2199–2207.
[13] Gustaf Ostberg, Katharina Buss, M. Christensen, S. Norgren, H. Andrén, Daniele Mari, G. Wahnstrom, I. Reineck, Mechanisms of plastic deformation of WC–Co and Ti(C,N)–WC–Co, Int. J. Refract. Met. Hard Mater. 24 (2006) 135–144.
[14] T. Sahraoui, A. Kellou, H.I. Faraoun, N. Fenineche, H. Aourag, C. Coddet, Ab initio calculations and experimental studies of site substitution of ternary elements in WC, Mater. Sci. Eng. B 107 (2004) 1–7.
[15] W.S. Young, I.B. Cutler, Initial sintering with constant rates of heating, J. Am. Ceram. Soc. 53 (1970) 659–663.
[16] Panigrahi Bharat, Sintering and grain growth kinetics of ball milled nanocrystalline nickel powder, Mater. Sci. Eng. A 460 (2007) 7–13.

[17] W.D. Kingery, H.K. Bowen, D.R. Uhlmann, Introduction to Ceramics, second ed., John Wiley and Sons, New York, 1975.
[18] R.L. Coble, Initial sintering of alumina and hematite, J. Am. Ceram. Soc. 41 (1958) 55–62.
[19] R.L. Coble, Sintering crystalline solids. I. Intermediate and final state diffusion models, J. Appl. Phys. 32 (1961) 787–792.
[20] R.L. Coble, Sintering crystalline solids. II. Experimental test of diffusion models in powder compacts, J. Appl. Phys. 32 (1961) 793–799.
[21] J.J. Bacmann, G. Cizeron, Dorn Method in the study of initial phase of uranium dioxide sintering, J. Am. Ceram. Soc. 51 (1968) 209–212.
[22] X. Wang, Z. Fang, H.Y. Sohn, Grain growth during the early stage of sintering of nanosized WC–Co powder, Int. J. Refract. Met. Hard Mater. 26 (2008) 232–241.
[23] C.P. Buhsmer, P.H. Crayton, Carbon self diffusion in tungsten carbide, J. Mater. Sci. 6 (1971) 981–988.
[24] G. Muginstein, S. Berger, A. Rosen, Sintering study of nanocrystalline WC powders, Nanostructured Mater. 10 (1998) 795–804.
[25] D. Demirskyi, A. Ragulya, D. Agrawal, Initial stage sintering of binderless tungsten carbide powder under microwave radiation, Ceram. Int. 37 (2011) 505–512.
[26] M.N. Rahman, Ceramic Processing and Sintering, second ed., M Dekker, New York, 2003.
[27] K.L. Johnson, Contact Mechanics, first ed., Cambridge University Press, UK, 1985.
[28] F.F. Lange, Sinterability of agglomerated powders, J. Am. Ceram. Soc. 67 (1984) 83–89.
[29] J. Gurland, Application of dihedral angle measurements to the microstructure of cemented carbides WC–Co, Metallography 10 (1977) 461–468.
[30] B.J. Kellett, F.F. Lange, Thermodynamics of densification. I. Sintering of simple particle arrays, equilibrium configurations, pore stability and shrinkage, J. Am. Ceram. Soc. 72 (1989) 725–741.